FLUCTUATIONS IN THE DIRECTION OF PROPAGATION OF LOW FREQUENCY IONOSPHERIC WAVES

Hiroatsu Sato[(1)], Hans L. Pécseli[(2)], Jan K. Trulsen[(3)]

[(1)]*University of Oslo, Physics Department, Box 1048 Blindern, N-0316 Oslo, Norway. Email: hiroatsu.sato@fys.uio.no*
[(2)]*University of Oslo, Physics Department, Box 1048 Blindern, N-0316 Oslo, Norway. Email: hans.pecseli@fys.uio.no*
[(3)]*University of Oslo, Institute of Theoretical Astrophysics, Box 1029 Blindern, N-0315 Oslo, Norway. Email: j.k.trulsen@astro.uio.no*

ABSTRACT

Low frequency electrostatic waves in the ionospheric E-region are studied using data obtained by an instrumented rocket. Restricting the analysis to low frequencies and long wavelengths we find that the direction of wave-propagation varies randomly within a wide interval of aspect angles. We found evidence for fluctuations, or ``jittering", of the direction of the local electric field vector. The distribution of the directional change per time unit is determined. The distribution is found to depend on the intensity of the turbulence indicating also a significant spatial intermittency of the signal. Large amplitude fluctuations have a narrow aspect-angle distribution with little directional fluctuations. The wave properties depend on the strength of the ambient DC-electric field.

1. INTRODUCTION

Low frequency longitudinal waves are often spontaneously excited in the ionospheric E-region, in the equatorial as well as the Polar Regions as detected first by radar scattering [1-4] and later by instrumented rockets [5-7].

The Farley-Buneman (FB) instability [2,8-10] excites low frequency electrostatic waves in the E-region of the Earth's ionosphere when the ambient electric field exceeds a certain threshold value, of the order of 20 mV/m. The instability is driven by the Hall-current in the collisional plasma typically found in the ionospheric E-region in the equatorial as well as the polar ionospheres, although the origin of this DC-electric field is generally different in the two regions. We have $\Omega_{ci} \leq \nu_{ni}$ and $\omega_{ce} \gg \nu_{ne}$, with electron and ion cyclotron frequencies ω_{ce} and Ω_{ci}, while the electron and ion neutral collision frequencies are ν_{ne} and ν_{ni}, respectively. The ions are in effect dragged by the neutrals while the electrons on the other hand move approximately with the $\boldsymbol{E}_0 \times \boldsymbol{B}_0/B_0^2$ - velocity. Assuming small growth-rates of the instability, a simplified fluid model gives a linear dispersion relation [11] where the real and imaginary parts of the frequency are

$$\omega_r = \frac{kV_d \cos\alpha}{1+\varphi} \qquad (1)$$

$$\omega_i = \frac{1}{1+\varphi}\left(\frac{\varphi}{\nu_{ni}}(\omega_r^2 - k^2C_s^2) + \frac{\omega_r \nu_{ni}}{kL_n\Omega_{ci}}\right) - 2\beta_r n_0, \qquad (2)$$

where β_r is a recombination coefficient,

$$\varphi = \frac{\nu_{ne}\nu_{ni}}{\omega_{ce}\Omega_{ci}}\left(1 + \frac{\omega_{ce}^2 k_\parallel^2}{\nu_{ne}^2 k^2}\right),$$

and L_n denotes the scale length of a possible large scale plasma density gradient in the direction $\perp \boldsymbol{B}_0$, while $\boldsymbol{V}_d$ is the difference between the electron and ion drift velocities, and α is the angle between $\boldsymbol{V}_d$ and $\boldsymbol{k}$. The analysis uses the quasi-neutrality assumption, and consequently the result only applies for wavelengths much longer than the Debye length, λ_D. The result (1)-(2) is valid in the limit of very small growth rates, $\omega_i \ll \omega_r$, and almost $\mathbf{B}_0$-perpendicular wave propagation, $k_\parallel \ll k_\perp$. We note that a gradient in plasma density contributes to instability at any drift velocity (last term in the parenthesis of (2)) provided it has the correct sign [3]. The relative drift between electrons and ions has to exceed the ion sound speed C_s in order to give Farley-Buneman unstable waves, otherwise the corresponding term has a damping effect. In this simple model, the first waves to become unstable are those where $\boldsymbol{k} \perp \boldsymbol{B}_0$. Since $\omega_{ce} \gg \nu_{ne}$ and $\Omega_{ci} \leq \nu_{ni}$ for the relevant ionospheric conditions, we find that waves with large $k_\parallel$ give large φ and therefore small ω_r, and will consequently remain linearly stable for realistic values of V_d. Recombination acts as a damping mechanism in all cases. For the relevant plasma conditions analyzed in the following, we can ignore large scale plasma density gradients $\perp \boldsymbol{B}_0$. Different models for the linearly unstable dispersion diagram have been compared [12]. We here gave emphasis to the FB and density gradient instabilities, but should mention that also other instabilities can be

Proc. '20th ESA Symposium on European Rocket and Balloon Programmes and Related Research'
Hyère, France, 22–26 May 2011 (ESA SP-700, October 2011)

operative in the ionospheric E-region, Kelvin-Helmholtz instabilities, for instance. These can be generated by shear in the neutral winds often prevailing in these regions. Finally one can not exclude the possibility that the space-craft itself can generate disturbances to be detected by the probes: such cases can be difficult to identify by a single space-craft.

The aim of the present study is to analyze the direction of the low frequency wave propagation as observed in the ionosphere [13]. Bulk variations in the direction of propagation with altitude were illustrated before [14] together with some earlier qualitative studies [15], but those results were obtained by a local cross correlation, which involves averaging over an altitude interval. Here we want to obtain results with the sampling resolution of the rocket instruments, and analyze also the time variations of the direction of the electric field vector. The present analysis is based on data from the ROSE rocket campaign [15,16]. This communication presents the first results of our analysis as outlined before, as carried out in the fixed rest frame, or ground frame, of reference.

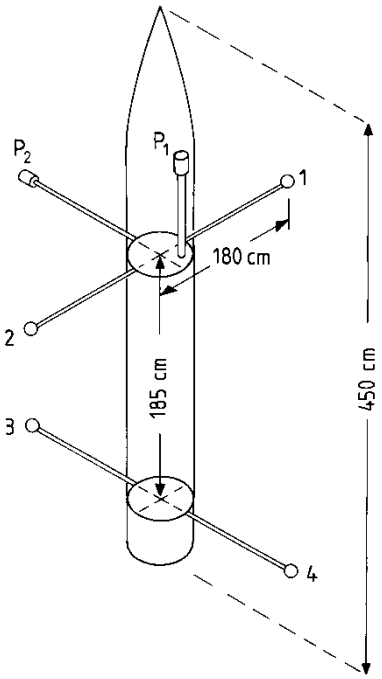

Figure 1. Schematic illustration for the positioning of probes on the ROSE4 rocket [16]. The nose cone is shown intact for illustration.

2. ELECTROSTATIC WAVES OBSERVED IN THE IONOSPHERIC E-REGION

During the ROSE rocket campaign [15,16], an instrumented payload F4 was launched in February 1989 from Kiruna, Sweden. The peak altitude was approximately 125 km. Good quality data were obtained on the up-leg as well as on the down-leg parts of the flight with approximately 20 km horizontal separation. The DC-electric field strength was changing during the flight (typically $\boldsymbol{E}_0 \approx 40$ mV/m up-leg, and $\boldsymbol{E}_0 \approx 60$ mV/m down-leg), so in reality we have data from two independent experiments. The direction and time-variation of $\boldsymbol{E}_0$ is illustrated elsewhere [14,15]. It was found that the *direction* of $\boldsymbol{E}_0$ was relatively constant; the changes were mostly in its amplitude. Numerical simulations of similar ionospheric conditions have also been carried out [12]. In this case a value of $\boldsymbol{E}_0 \approx 70$ mV/m was chosen to emphasize the nonlinear effects.

For completeness we here summarize some of the basic parameters of the flight and the instrumentation. The ROSE F4 rocket was launched in a direction perpendicular to the Hall current of the electrojet. The spin period of the rocket was approximately 0.5 s. The corresponding time for the coning motion was approximately 6 s with cone-angle approximately 2°. The effects of the coning of the rocket can thus be ignored. The rocket payload flew northward. On the upleg part the trajectory made an angle of approximately 30° with respect to the Earth's magnetic field, and was almost parallel with $\boldsymbol{B}$ on the downleg part [15].

The ELF signals analyzed were obtained by gold-plated spherical probes of 5 cm diameter [15], mounted on two pairs of booms, one near the top of the payload (labeled 1 and 2) and the other a distance L = 185 cm lower (labeled 3 and 4), oriented at an angle of 90° with respect to the first pair, as illustrated schematically in Fig. 1. The length of each boom was b = 180 cm, giving a probe separation of 360 cm on each boom. We analyzed the fluctuating signals $U_6(t) = \phi_1(t) - \phi_2(t)$; $U_5(t) = \phi_4(t) - \phi_3(t)$; $U_4(t) = \phi_1(t) - \phi_4(t)$; $U_3(t) = \phi_2(t) - \phi_3(t)$; $U_2(t) = \phi_1(t) - \phi_3(t)$; and $U_1(t) = \phi_2(t) - \phi_4(t)$, where $\phi_j(t)$ for $j = 1, 2, 3, 4$ denotes the potential on the j-th probe with respect to a suitably defined common ground. There is a redundancy in the available signals, which can be used to check the performance of individual probes. For wavelengths much larger than the probe separations, the potential difference signals can be used to estimate the fluctuating electric fields, $\boldsymbol{E}$. The signals were digitized with 12 bit resolution. The space-time varying electric field fluctuations of the electrojet were originally sampled with a 4 kHz sampling frequency. By averaging sampling points two-by-two, we increase the sampling interval to 0.5 ms, giving a Nyquist frequency of 1000 Hz. The electric circuits give an effective frequency limitation closer to 600 Hz. The DC-electric field $\boldsymbol{E}_0$ was measured by the same probes.

We use a combination of probes to approximate the three electric field components. Thus $U_6/2b$ approximates *x*-component, $U_5/2b$ the *y*-component, and $(U_3 + U_4)/2L$ approximates the *z*-component of the field. For constant electric fields these signals would recover the field-components exactly. For wavelengths longer than the probe separations (as in the present case), we expect this probe combination to give a good approximation for the magnitude and direction of the fluctuating electrostatic field.

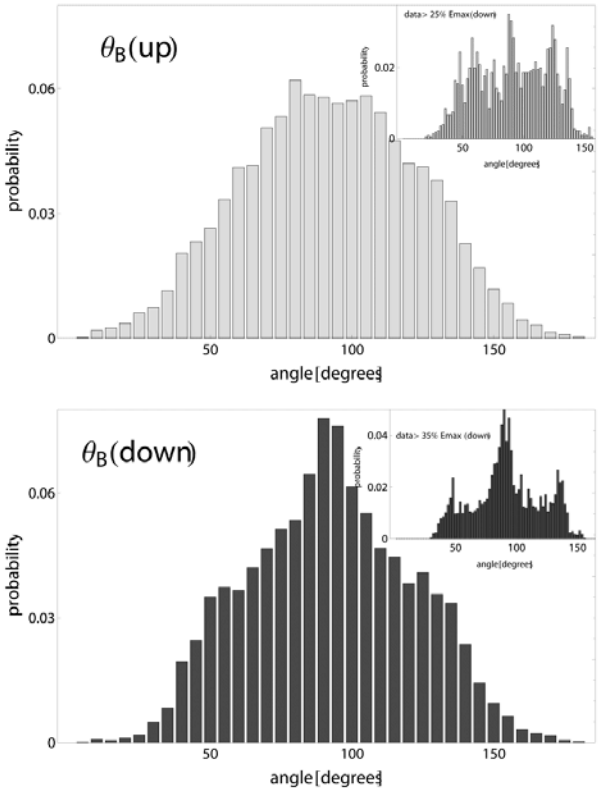

.

Figure 2. Probability densities of the angle between the electric field vector with respect to $\boldsymbol{B}_0$*, for up-leg and down-leg conditions. The figures shown in the inserts are obtained by imposing conditions on the detected field amplitudes.*

Studies of the ROSE F4 data demonstrated that a broad band spectrum of low frequency electrostatic waves propagate in the $\boldsymbol{E}_0 \times \boldsymbol{B}_0$-direction with a phase velocity in the range of 250 – 400 m/s. The observed frequency range is 5 – 1000 Hz, implying wavelengths in the range of 0.25 – 80 m. The shortest wavelengths are strongly filtered by the two-point probe sampling of the fluctuating electrostatic fields [14,17,18]. The data approximate the fluctuating electric fields only when the wavelengths significantly exceed the probe separation (see Fig. 1), which here corresponds to frequencies below 28 Hz, approximately. We filter the data correspondingly, and consider only a limited spectral range. (In related previous studies [15], the speed of propagation was not known, and too short wavelengths, i.e. too high frequencies, were included in the data analysis.) We filter the data with a band-pass filter {8:28} Hz, whereby we at the same time remove the rocket spin frequency and its first harmonics, and also ensured that the filter-bandwidth is larger than its average frequency. In case this condition is not fulfilled, the time variability of the output will be determined by the filter characteristics and not the ionospheric signal. Due to the filtering, the present data-set does not contain the ambient electric field $\boldsymbol{E}_0$, nor the $\boldsymbol{V}_R \times \boldsymbol{B}_0$-field, with $\boldsymbol{V}_R$ being the rocket velocity. The variations in magnitude and direction of $\boldsymbol{E}_0$ during the flight are illustrated elsewhere [15].

The electric fields are detected in the rest frame of the rocket. To have the direction in the fixed frame, the data are transformed to a fixed ground frame by use of transformation and rotation matrices. The change in frame of reference is obtained by several such matrix operations. The *z*-axis is taken to be parallel to the ambient magnetic field.

In Fig. 2 we show the probability density of angles between the electric field vector for the spectral range defined before, as measured with respect to the magnetic field, both for up-leg and down-leg conditions.

For electrostatic waves the direction of the electric field corresponds to the direction of the wave propagation so we can identify a local direction of propagation with the direction of the electric field.

We can obtain results for the directional change with respect to a fixed direction in space, which for these ionospheric conditions is taken to be along $\boldsymbol{B}_0$. The probability density for the variation in electric field direction $\Delta\theta_B$ with respect to $\boldsymbol{B}_0$ from one sampling time step to the next is shown in figure 3.

We can analyze also the changes in direction between $\boldsymbol{E}(t)$ and $\boldsymbol{E}(t+\Delta t)$. The temporal relative variation of the direction of propagation is obtained from the data by the simple formula

$$\Delta\theta_E = ArcCos\left(\frac{\boldsymbol{E}(t)\cdot\boldsymbol{E}(t+\Delta t)}{|E(t)||E(t+\Delta t)|}\right), \quad (3)$$

giving the change in $\theta_E(t)$ within one sampling time interval, Δt. With Δt being small compared to characteristic times for changes in θ_E, we can approximate $\boldsymbol{E}(t+\Delta t) \approx \boldsymbol{E}(t) + \Delta t\ (d\boldsymbol{E}(t)/dt)$, and simplify (3) by a series expansion, which can be used for analytical estimates.

The results for the distribution of θ_E between two directions $\boldsymbol{E}(t)$ and $\boldsymbol{E}(t + \Delta t)$ are shown in Fig. 4. We find that the most probable change in electric field direction within a time interval $\Delta t = 10^{-3}$ s is 2˚- 3˚. For large values of $\Delta\theta_E$, both probability densities can be fitted to a good accuracy by an exponential exp(-$\Delta\theta_E/\Lambda$). We find the approximate values $\Lambda = 2.86^{\circ}$ and 3.04° for up-leg and down-leg conditions.

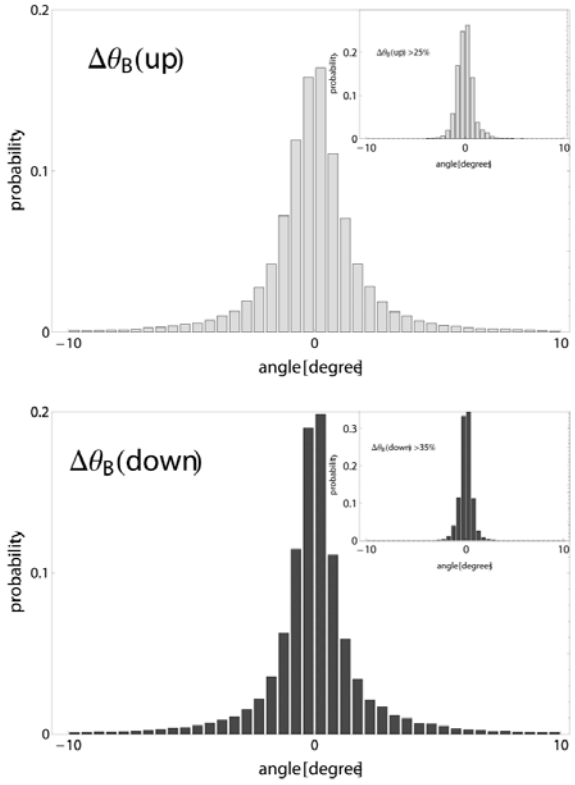

Figure3. Probability densities of the changes in direction of propagation of low frequency electrostatic waves in the ionospheric E-region in the fixed frame of reference. The figure shows the change in direction $\Delta\theta_B$ *with respect to the magnetic field lines within one sampling time* Δt*. To obtain the approximation* $d\theta_B/dt \approx \Delta\theta_B/\Delta t$*, we divide the abscissa values by* $\Delta t = 10^{-3}$ *s.*

To investigate whether observed variations were related to the electric field amplitude we performed a cross correlation between the electric field amplitude and $\Delta\theta_B$, obtaining the values 0.32 and 0.38 for up-leg and down-leg conditions, respectively. This is a nontrivial correlation, which seems to be largest when the ambient electric field E_0 is largest. To test that the finite record length is insignificant for these results we made a test by random number generators, producing synthetic data samples of same length. In this case we found a typical correlation coefficient of the order of 10^{-3}, demonstrating that our results are robust.

3. INTERMITTENT FEATURES OF THE FLUCTUATING ELECTRIC FIELDS

Our basic analysis considers the unconditional electric field direction, i.e. irrespective of the magnitude of |**E**|. It is known that the signal has significantly intermittent features [19], with localized bursts of intense wave activity intermixed with somewhat more quiescent regions, as illustrated in Fig. 5 showing a sample of $|\boldsymbol{E}(t)|$. The intermittent features are most pronounced for the down-leg part of the flight.

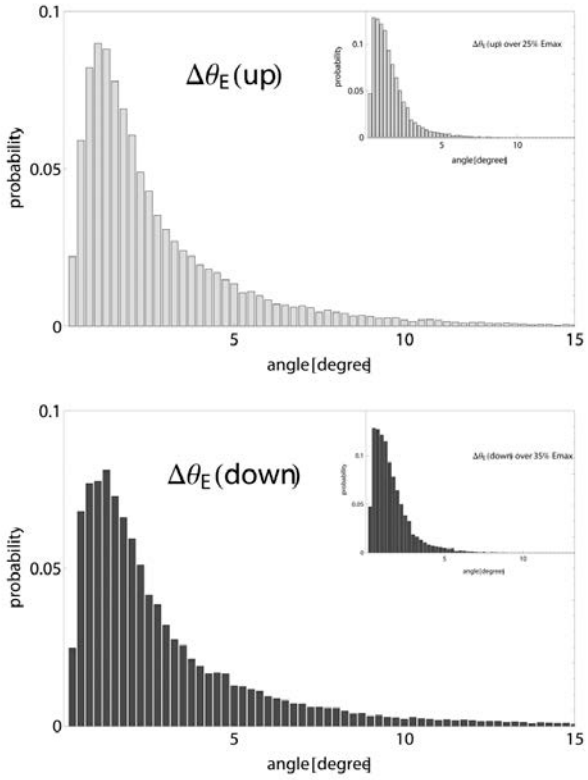

Figure 4. Probability densities of the changes in direction of propagation of low frequency electrostatic waves in the ionospheric E-region. The figure shows $\Delta\theta_E$ *in degrees, as obtained by (3). To obtain the approximation* $d\theta_E/dt \approx \Delta\theta_E/\Delta t$*, we divide the abscissa values by* $\Delta t = 10^{-3}$ *s.*

The results of our analysis changes noticeably if we impose conditions on the magnitude of |**E**|, as illustrated by inserts in Figs. 2, 3 and 4, where we removed the smallest 35 % of the |**E**|-values from the analysis (25 % for the upleg part). Now we observe a central peak (seen best on the down-leg part where E_0 was largest) with a moderate aspect angle variation, and an additive distribution of large aspect angle waves. We expect that the central peak represents the Farley-Buneman waves, where both radar [20] and laboratory results [21] give a narrow distribution of aspect angles. Our result for the down-leg part shows a half-width of this central peak

distribution of approximately 7˚ which is close to previous results [20,22]. Similar results are obtained for the up-leg part of the flight (see Fig. 2), although for this reduced value of E_0 the results are not quite as clear. The time variability of the electric field directions with amplitudes exceeding the 35 % threshold values is also reduced, as evidenced by the inserts in Figs. 3 and 4. This implies that any detection method involving time integration is likely to miss the low amplitude fluctuations, and emphasize the central peak here associated with waves generated by the Farley-Buneman instability. By a Monte-Carlo analysis we find that the angular width obtained by our results is most likely limited by the finite probe separation on the rocket (see Fig. 1), so that the actual angular distribution is likely to be narrower.

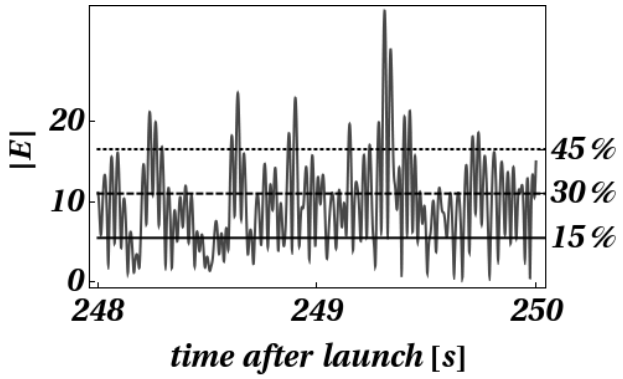

Figure. 5. Illustration of the amplitude-clipping applied for the intermittency studies. Note that the electrostatic waves detected in the ionospheric E-region are not linearly polarized, so it is only rarely that we find the electric field amplitude $|\boldsymbol{E}| = 0$.

We demonstrated also a significant intermittency of the E-region fluctuations: the large amplitude regions contain a significant narrow aspect angle component, which is much less conspicuous in the low amplitude regions. The largest amplitude waves thus seem concentrated into relatively narrow layers that are randomly distributed in altitude. These observation are consistent with the bispectral analysis of the same data as reported before [12,23], where the local bicoherences were found to be of a ``bursty" nature, concentrated to localized regions. Our results were compared to analytical results for Gaussian random processes, and we confirmed that the intermittency effects observed here originate from non-Gaussian features.

4. DISCUSSIONS AND CONCLUSIONS

In the present study we analyzed the direction of low frequency, long wavelength, electric fields excited in the ionospheric E-region by a cross-field instability. We found that the most probable propagation direction is perpendicular to $\boldsymbol{B}_0$, both for up-leg and down-leg conditions, but note also that deviations in directions as large as 50˚ have a significant probability of occurrence. The direction of the average wave propagation is, within the uncertainty of the estimate, normal to the DC-electric field [15].

By a conditional analysis, removing the smallest 25 % - 35 % of the electric field amplitudes, we obtained a two-component directional distribution with a central peak here identified with the waves generated by the FB instability. The other component with a wide aspect angle distribution is most likely generated by a different instability, although we are aware of models predicting wide angle distributions for the saturated stage of the FB-instability [24]. A pronounced altitude variation of the propagation velocity was observed for the ROSE F4 data [14], with velocities starting at a value close to the sound speed, but decreasing to noticeably smaller velocities. There are no altitude variations of plasma parameters to explain this variation [14]. In comparison, the propagation velocity obtained by a Greenland rocket [25] under somewhat similar conditions, did not show any significant altitude variation. No significant DC-plasma density variations were detected by the ROSE instruments, so we discard the possibility of density gradient drift waves. The most plausible cause of the altitude variations in the observed propagation velocity is an altitude variation of the neutral wind velocity. The corresponding shear can be a mechanism for generating the waves with wide aspect angle distributions.

Our results indicate a significant intermittency of the long wavelength part of the FB instability, where previous studies [19] refer to the short wavelength part.

Our observations demonstrate a clear difference between the results for up-leg and down-leg conditions. The most significant parameter difference between these two cases is the value of the ambient DC-electric field $\boldsymbol{E}_0$. The rms-fluctuation level varies consistently with $|\boldsymbol{E}_0|$ as demonstrated previously [14,26]. In the present study we have demonstrated that the direction of propagation as determined by the time varying electrostatic field is fluctuating, and found also these fluctuations to be strongest when $|\boldsymbol{E}_0|$ was large. The results can have importance for interpreting the wave vector matching conditions in radar backscatter from instabilities in the ionospheric E-region, for instance.

ACKNOWLEDGMENTS

The Rocket and Scatter Experiment (ROSE) was performed in the framework of the German national sounding rocket program with international participation. It was primarily funded by the Bundes-ministerium für Forschung und Technologie (BMFT) and was managed by the Deutsche Gesellschaft für

Luft- und Raumfahrt (DLR). The present study was supported in part by a grant from the Norwegian National Science Foundation. The authors thank Jean-Pierre St-Maurice for valuable comments.

5. REFERENCES

1. Olesen, J. K. and Rybner, J., In *AGARDograph*, Ionospheric Research Meeting, 37–57, Cambridge, England, September 1958. AGARD Avionics Panel.
2. Bowles, K. L., Cohen, R., and Balsley, B. B., *J. Geophys. Res.*, Vol. 68, 2485–2501, 1963.
3. Balsley B. B., *J. Geophys. Res.*, Vol. 74, 2333–2347, 1969.
4. Olesen, J. K.., In *Radar propagation in the arctic, specialists meeting of the electromagnetic wave propagation*, AGARD-CP-97, page 27, Lindau/Harz, FRG, 13-17, September 1971. Max Planck-Institut für Aeronomie.
5. Prakash, S., Gupta, S. P., Subbaray, B. H., and Jain, C. L., *Nature-Physical Sciences*, Vol. 233, 56-58, 1971.
6. Olesen, J. K., Primdahl, F., Spangslev, F., Ungstrup, E., Bahnsen, A., Fahleson, U., Fälthammar, C.-G., and Pedersen, A., *Geophys. Res. Lett*., Vol. 3, 711–714, 1976.
7. Pfaff, R. F., Kelley, M. C., Fejer, B. G., Maynard, N. C., Brace, L. H., Ledley, B. G., Smith, L. G., and Woodman, R. F., *J. Atmos. Terr. Phys.*, Vol. 47, 791–811, 1985.
8. Farley, D. T., *Phys. Rev. Lett.*, Vol. 10, 279–282, 1963.
9. Buneman, O., *Phys. Rev. Lett.*, Vol. 10, 285–287, 1963.
10. Kelley, M. C., *The Earth's Ionosphere, Plasma Physics and Electrodynamics*,Vol. 43 of International Geophysics Series. Academic Press, San Diego, California, 1989.
11. Fejer, B. G., Providakes, J., and Farley, D. T., *J. Geophys. Res.*, Vol. 89, 7487–7494, 1984.
12. Dyrud, L., Krane, B., Oppenheim, M., Pécseli, H. L., Schlegel, K., Trulsen, J., and Wernik, A. W., *Ann. Geophys.*, Vol. 24, 2959–2979, 2006.
13. Pfaff, R. F., Marionni, P. A., and Swartz, W. E., *Geophys. Res. Lett.*, Vol. 24, 1663–1666, 1997.
14. Krane, B., Pécseli, H. L., Trulsen, J., and Primdahl, F., *J. Geophys. Res*., Vol. 105, 10585–10601, 2000.
15. Rinnert, K., *J. Atmos. Terr. Phys.*, Vol. 54, 683–692, 1992.
16. Rose, G., Schlegel, K., Rinnert, K., Kohl, H., Nielsen, E., Dehmel, G., Friker, A., Lubken, F. J., Lühr, H., Neske, E., and Steinweg, A., *J. Atmos. Terr. Phys.*, Vol. 54, 657–667, 1992.
17. Kelley, M. C. and Mozer, F. S., *J. Geophys. Res.*, Vol. 78. 2214–2221, 1973.
18. Pfaff, R. F., Kelley, M. C., Fejer, B. G., Kudeki, E., Carlson, C. W., Pedersen, A., and Hausler, B., *J. Geophys. Res.*, Vol. 89, 236–244, 1984.
19. Dyrud, L., Krane, B., Oppenheim, M., Pécseli, H. L., Trulsen, J., and Wernik, A. W., *Nonlin. Processes Geophys.*, Vol. 15, 847–862, 2008.
20. Jackel, B. J., Moorcroft, D. R., and Schlegel, K.., *Ann. Geophysicae*, Vol. 15, 54–62, 1997.
21. Alport, M. J., D'Angelo, N., and Pécseli, H. L., *J. Geophys. Res.*, Vol. 86, 7694–7702, 1981.
22. Jackel, B. J., Moorcroft, D. R, Foster, J. C., and Schlegel, K.., *J. Geophys. Res.*, Vol. 107, 1122, 2002.
23. Larsen, Y., Hanssen A., Krane B., Pécseli H. L., and Trulsen J., *J. Geophys. Res.*, Vol. 107, 1005, 2002, doi:10.1029/2001JA900125.
24. Drexler, J. and St. Maurice, J. P., *Ann. Geophysicae*, Vol. 23, 767–772, 2005.
25. Pécseli, H. L., Primdahl, F., and Bahnsen, A.. *J. Geophys. Res.*, Vol. 94, 5337–5349, 1989.
26. Iranpour, K., Pécseli, H. L., Trulsen, J., Bahnsen, A., Primdahl, F., and Rinnert, K., *Ann. Geophysicae.*, Vol. 15, 878, 1997.